Encyclopedia of Mathematical Physics EMP MS 93 October 21, 2004,

Chaos and Attractors

Robert Gilmore
Physics Department, Drexel University, Philadelphia, PA 19104

1 Introduction

Chaos is a type of behavior that can be exhibited by a large class of physical systems and mathematical models of them. These systems are deterministic. They are modeled by sets of coupled nonlinear ordinary differential equations (ODEs)

$$\dot{x}_i = \frac{dx_i}{dt} = f_i(x;c) \tag{1}$$

called dynamical systems. The coordinates x designate points in a state space or phase space. Typically $x \in R^n$ or some n-dimensional manifold for some $n \geq 3$, and $c \in R^k$ are called control parameters. They describe parameters that can be controlled in physical systems, such as pumping rates in lasers or flow rates in chemical mixing reactions. The most important mathematical property of dynamical systems is the uniqueness theorem which states that there is a unique trajectory through every point at which $f(x;c) \neq 0$. In particular, two distinct periodic orbits cannot have any points in common.

The properties of dynamical systems are governed, in lowest order, by the number, stability, and distribution of their fixed points, defined by $\dot{x}_i = f_i(x;c) = 0$. It can happen that a dynamical system has no stable fixed points and no stable limit cycles [$x(t) = x(t+T)$, some $T > 0$, all t]. In such cases, if the solution is bounded and recurrent but not periodic, it represents an unfamiliar type of attractor. If the system exhibits "sensitivity to initial conditions" [$|x(t) - y(t)| \sim e^{\lambda t}|x(0) - y(0)|$ for $|x(0) - y(0)| = \epsilon$ and $\lambda > 0$ for most $x(0)$] the solution set is called a "chaotic attractor." If the attractor has fractal structure it is called a "strange attractor."

Tools have been developed to study strange attractors that depend on three types of mathematics:

- geometry
- dynamics
- topology

Geometric tools attempt to study the metric relations among points in a strange attractor. These include a spectrum of fractal dimensions. These real numbers are difficult to compute, require very long, very clean data sets, provide a number without error estimates for which there is no underlying statistical theory, and provide very little information about the attractor.

Dynamical tools include estimation of Lyapunov exponents and a Lyapunov dimension. They include globally averaged exponents and local Lyapunov exponents. These are eigenvalues related to the different stretching ($\lambda > 0$) and squeezing ($\lambda < 0$) eigendirections in the phase space. To each globally averaged Lyapunov exponent λ_i, $\lambda_1 \geq \lambda_2 \geq \ldots \geq \lambda_n$ there corresponds a "partial dimension" ϵ_i, $0 \leq \epsilon_i \leq 1$, with $\epsilon_i = 1$ if $\lambda_i \geq 0$. The Lyapunov dimension is the sum of the partial dimensions $d_L = \sum_{i=1}^{n} \epsilon_i$. That the partial dimension $\epsilon_i = 1$ for $\lambda_i \geq 0$ indicates that the flow is smooth in the stretching ($\lambda_i > 0$) and flow directions and fractal in the squeezing ($\lambda_i < 0$) directions

with $\epsilon_i < 1$. Dynamical indices provide some useful information about a strange attractor. In particular, they can be used to estimate some fractal properties of a strange attractor, but not vice versa.

Topological tools are very powerful for a restricted class of dynamical systems. These are dynamical systems in three dimensions ($n = 3$). For such systems there are three Lyapunov exponents $\lambda_1 > \lambda_2 > \lambda_3$, with $\lambda_1 > 0$ describing the stretching direction and responsible for "sensitivity to initial conditions," $\lambda_2 = 0$ describing the direction of the flow, and $\lambda_3 < 0$ describing the squeezing direction and responsible for "recurrence." Strange attractors are generated by dissipative dynamical systems, which satisfy the additional condition $\lambda_1 + \lambda_2 + \lambda_3 < 0$. For such attractors $\epsilon_1 = \epsilon_2 = 1$ and $\epsilon_3 = \lambda_1/|\lambda_3|$ by the Kaplan-Yorke conjecture, so that $d_L = 2 + \epsilon_3 = 2 + \lambda_1/|\lambda_3|$.

A number of tools from classical topology have been exploited to probe the structure of strange attractors in three dimensions. These include: the Gauss linking number; the Euler characteristic; the Poincaré-Hopf index theorem; and braid theory. More recent topological contributions include: several definitions for entropy; the development of a theory for knot holders or braid holders (also called branched manifolds); the Birman-Williams theorem for these objects; and relative rotation rates, a topological index for individual periodic orbits and orbit pairs.

Three dimensional strange attractors are remarkably well understood. Those in higher dimensions are not. As a result, the description that follows is largely restricted to strange attractors with $d_L < 3$ that exist in R^3 or other three-dimensional manifolds (e.g., $R^2 \times S^1$). The obstacle to progress in higher dimensions is the lack of a higher-dimensional analog of the Gauss linking number for orbit pairs in R^3.

2 Overview

The program described below has two objectives:

- Classify the global topological structure of strange attractors in R^3;
- Determine the perestroikas that such attractors can undergo as experimental conditions or control parameters change.

Four levels of structure are required to complete this program. Each is topological. Each is discretely quantifiable. This provides a beautiful interaction between a rigidity of structure, demanded by topological constraints, and freedom within this rigidity. These four levels of structure are:

1. Basis sets of orbits
2. Branched manifolds or Knot holders
3. Bounding tori
4. Embeddings of bounding tori.

3 Branched Manifolds: Stretching and Squeezing

A strange attractor is generated by the repetition of two mechanisms: stretching and squeezing. Stretching occurs in the directions identified by the positive Lyapunov exponents and squeezing occurs in the directions identified by the negative Lyapunov exponents. In R^3 there is one stretching direction and one squeezing direction.

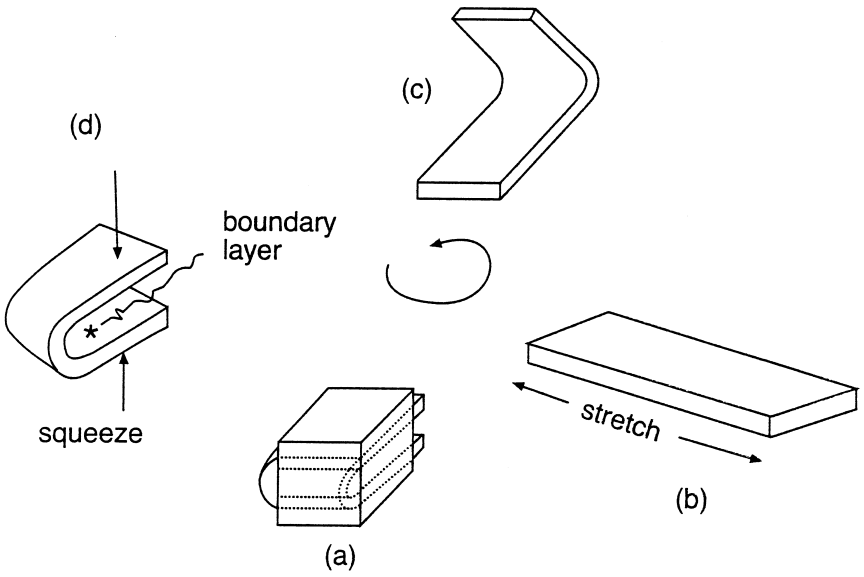

Figure 1: A common stretch and fold mechanism generates many experimentally observed strange attractors. Reprinted with permission from R. Gilmore and M. Lefranc, *The Topology of Chaos*, NY: Wiley, 2002.

A simple stretch and squeeze mechanism that Nature appears very fond of is illustrated in Fig. 1. In this illustration, a cube of initial conditions at (a) is advected by the flow in a short time to (b). During this process the cube is deformed by being stretched ($\lambda_1 > 0$). It also shrinks in a transverse direction ($\lambda_3 < 0$). During the initial phase of this deformation two nearby points typically separate exponentially in time. If they were to continue to separate exponentially for all times the invariant set would not be bounded. Therefore this separation cannot continue indefinitely, and in fact it must somehow reverse itself after some time because the motion is recurrent. The mechanism shown in Fig. 1 involves folding, which begins between (b) and (c) and continues through to (d). Squeezing occurs where points from distant parts of the attractor approach each other exponentially, as at (d). Finally the cube, shown deformed at (d), returns to the neighborhood of initial conditions (a). This process repeats itself and builds up the strange attractor. As can be inferred from this figure, the strange attractor constructed by the repetitive process is smooth in the expanding (λ_1) and flow ($\lambda_2 = 0$) directions but fractal in the squeezing (λ_3) direction. The attractor's fractal dimension is $\epsilon_1 + \epsilon_2 + \epsilon_3 = 2 + \epsilon_3 = 2 + \lambda_1/|\lambda_3|$.

Figure 1 summarizes the boundedness and recurrence conditions that were introduced to define strange attractors, and illustrates one stretching and squeezing mechanism that occurs repetitively to build up the fractal stsructure of the strange attractor and to organize all the (unstable) periodic orbits in it in a unique way. The particular mechanism shown in Fig. 1 is called a stretch and fold mechanism. Other mechanisms involve stretch and roll, and tear and squeeze.

The stretch and squeeze mechanisms are well summarized by the cartoons shown in Fig. 2. On the left a cube of initial conditions (top) is deformed under the flow. The flow is downward. Stretching occurs in one direction (horizontal) and shrinking occurs in a transverse direction (perpendicular to

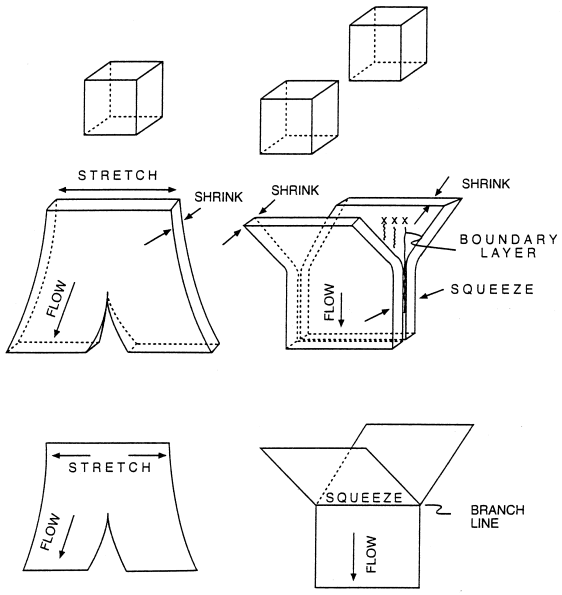

Figure 2: Left: The stretch mechanism is modeled by a two-dimensional surface with a splitting point singularity. Right: The squeeze mechanism is modeled by a two-dimensional surface with a branch line singularity. Reprinted with permission from R. Gilmore and M. Lefranc, *The Topology of Chaos*, NY: Wiley, 2002.

the page). In the limit of extreme shrinking ($\lambda_3 \to -\text{“}\infty\text{”}$) the dynamics of the stretching part of the flow is represented by the two-dimensional surface shown on the bottom left. This surface fails to be a manifold because of the singularity, called a splitting point. This singularity represents an initial condition that flows to an unstable fixed point with at least one stable direction. On the right (squeezing) two distant cubes of initial conditions (top) in the flow are deformed and brought to each other's proximity under the flow (middle). In the limit of extreme dissipation, two two-dimensional surfaces representing inflows are joined at a branch line to a single surface representing an outflow. This surface fails to be a manifold because of the branch line, which is a singularity of a different kind. Points below the branch line in this representation of the flow (on the outflow side of the branch line) have two preimages above the branch line, one in each inflow sheet. This structure generates positive entropy.

A beautiful theorem of Birman and Williams justifies the use of the two cartoons shown at the bottom of Fig. 2 to characterize strange attractors in R^3. As preparation for the theorem, Birman and Williams introduced an important identification for the nongeneric or atypical points that "are not sensitive to initial conditions"

$$x \sim y \qquad \text{if} \qquad |x(t) - y(t)| \stackrel{t\to\infty}{\longrightarrow} 0 \tag{2}$$

That is, two points in a strange attractor are identified if they have asymptotically the same future. In practice, this amounts to projecting the flow down along the stable ($\lambda_3 < 0$) direction onto a two dimensional surface described by the stretching ($\lambda_1 > 0$) and the flow ($\lambda_2 = 0$) directions. This

surface is not a manifold because of lower dimensional singularities: splitting points and branch lines. The two-dimensional surface has many names: knot holder (because it holds the periodic orbits that exist in abundance in strange attractors); braid holders; templates; branched manifolds. The flow, restricted to this surface, is called a semiflow. Under the semiflow, points in the branched manifold have a unique future but do not have a unique past. The degree of nonuniqueness is measured by the topological entropy of the dynamical system.

The Birman-Williams theorem is:

Theorem: Assume that a flow Φ_t

- on R^3 is dissipative ($\lambda_1 > 0, \lambda_2 = 0, \lambda_3 < 0$ and $\lambda_1 + \lambda_2 + \lambda_3 < 0$)
- Generates a hyperbolic strange attractor (the eigenvectors of the local Lyapunov exponents $\lambda_1,\ \lambda_2,\ \lambda_3$ span everywhere on the attractor).

Then the projection (2) maps the strange attractor $\mathcal{SA}$ to a branched manifold $\mathcal{BM}$ and the flow Φ_t on $\mathcal{SA}$ to a semiflow $\hat{\Phi}_t$ on $\mathcal{BM}$ in R^3. The periodic orbits in $\mathcal{SA}$ under Φ_t correspond 1:1 with the periodic orbits in $\mathcal{BM}$ under $\hat{\Phi}_t$ with perhaps one or two specified exceptions. On any finite subset of orbits the correspondence can be taken via isotopy.

The beauty of this theorem is that it guarantees that a flow Φ_t that generates a (fractal) strange attractor $\mathcal{SA}$ can be continuously deformed to a new flow $\hat{\Phi}_t$ on a simple two-dimensional structure $\mathcal{BM}$. During this deformation periodic orbits are neither created nor destroyed. The uniqueness theorem for ODEs is satisfied during the deformation so orbit segments do not pass through each other. As a result, the topological organization of all the unstable periodic orbits in the strange attractor is the same as the topological organization of all the unstable periodic orbits in the branched manifold. In fact, the branched manifold (knot holder) defines the topological organization of all the unstable periodic orbits that it supports. Topological organization is defined by the Gauss linking number and the relative rotation rates, another braid index.

The significance of this theorem is that strange attractors can be characterized — in fact classified — by their branched manifolds. Figure 3 shows a branched manifold "for a figure 8 knot" as well as the figure 8 knot itself (heavy curve). If a constant current is sent through a conducting wire tied into the shape of a figure 8 knot, a discrete countable set of magnetic field lines will be closed. These closed field lines can be deformed onto the two dimensional surface that is shown in Fig. 3. Each of the eight branches of this branched manifold can be named. One way to do this specifies the two branch lines that are joined by the branch in the sense of the flow: for example $(a\alpha)$ and $(\beta\alpha)$ (but not $(a\beta)$). Every closed field line can be labeled by a symbol sequence that is unique up to cyclic permutation. This symbol sequence provides a symbolic name for the orbit. For example $(a\alpha)(\alpha\beta)(\beta b)(ba)$ is a period-four orbit. The structure of a branched manifold is determined in part by a transition matrix T. The matrix element T_{ij} is 1 if the transition from branch i to branch j is allowed, 0 otherwise. The transition matrix for the figure 8 branched manifold is shown in Fig. 3.

The Birman-Williams theorem is stronger than its statement. More systems satisfy the statement of the theorem than satisfy the assumptions of the theorem. The figure 8 knot and its attendant magnetic field is not dissipative — in fact, it isn't even a dynamical system, yet the closed loops can be isotoped to the figure 8 knot holder. There are other ways the Birman-Williams theorem is stronger than its statement.

It is apparent from Fig. 3 that the figure 8 branched manifold can be built up Lego© fashion from the two basic building blocks shown in Fig. 2. This is more generally true. Every branched manifold can be built up, Lego© fashion, from the stretch (with a splitting point singularity) and the squeeze (with a branch line singularity) building blocks, subject to the two conditions:

1. outputs flow to inputs

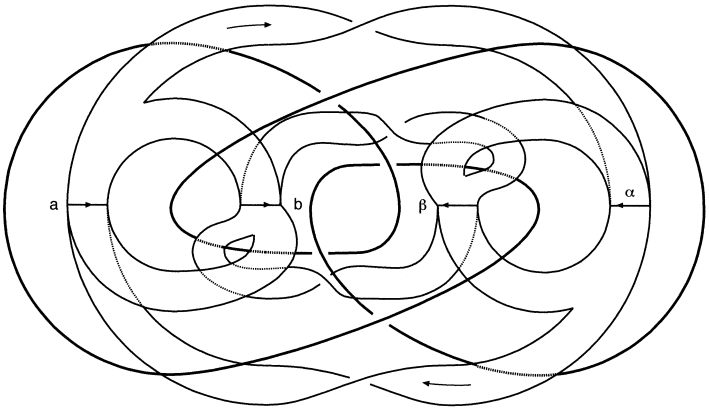

	ab	$a\alpha$	$\alpha\beta$	αa	ba	$b\beta$	$\beta\alpha$	βb
ab	0	0	0	0	1	1	0	0
$a\alpha$	0	0	1	1	0	0	0	0
$\alpha\beta$	0	0	0	0	0	0	1	1
αa	1	1	0	0	0	0	0	0
ba	1	1	0	0	0	0	0	0
$b\beta$	0	0	0	0	0	0	1	1
$\beta\alpha$	0	0	1	1	0	0	0	0
βb	0	0	0	0	1	1	0	0

Figure 3: Figure 8 knot (dark curve) and the figure 8 branched manifold. Transition matrix for the eight branches of the figure 8 branched manifold. Flow direction is shown by arrows. Reprinted with permission from R. Gilmore and M. Lefranc, *The Topology of Chaos*, NY: Wiley, 2002.

Table 1: Four sets of equations that generate strange attractors.

Dynamical System	Ordinary Differential Equations	Parameter Values
Rossler	$\dot{x} = -y - z$ $\dot{y} = x + ay$ $\dot{z} = b + z(x - c)$	$(a, b, c) = (2.0, 4.0, 0.398)$
Duffing	$\dot{x} = y$ $\dot{y} = -\delta y - x^3 + x + A\sin(\omega t)$	$(\delta, A, \omega) = (0.4, 0.4, 1.0)$
van der Pol	$\dot{x} = by + (c - dy^2)x$ $\dot{y} = -x + A\sin(\omega t)$	(b, c, d, A, ω) $=$ $(0.7, 1.0, 10.0, 0.25, \pi/2)$
Lorenz	$\dot{x} = -\sigma x + \sigma y$ $\dot{y} = Rx - y - xz$ $\dot{z} = -bz + xy$	$(R, \sigma, b) = (26.0, 10.0, 8/3)$

2. there are no free ends.

The figure 8 branched manifold is built up from four stretch and four squeeze building blocks. As a result, there are eight branches and four branch lines.

Two often studied strange attractors are shown in Figs. 4 and 5. Fig. 4 shows (a) the Rössler equations, (b) portions of the time traces $z(t)$ and $x(t)$, and (c) the projection of the strange attractor down onto the x-y plane. In the lower row are shown (d) a caricature of the flow, and (e) the knot holder for the flow. A similar spectrum of features is shown in Fig. 5 for the Lorenz equations. The knot holder in Fig. 5(e) is obtained from the caricature in Fig. 5(d) by twisting the right-hand lobe by π radians.

Branched manifolds can be used to characterize all three dimensional strange attractors. Branched manifolds that classify the strange attractors generated by four familiar sets of equations (for some control parameter values) are shown in Fig. 6. The sets of equations, and one set of parameter values that generate strange attractors, are presented in Table 1.

The beauty of this topological classification of strange attractors is that it is apparent, just by inspection, that there is no smooth change of variables that will map any of these systems to any of the others for the parameter values shown.

Branched manifolds can be described algebraically. In Fig. 7 we provide the algebraic description of two branched manifolds. In Fig. 7(a) we show the branched manifold that describes experimental data generated by many physical systems. The mechanism is a simple stretch and fold deformation with zero global torsion that generates a typical Smale horseshoe. There are two branches. The diagonal elements of the matrix identify the local torsion of the flow through the corresponding branch, measured in units of π. Branch 0 has 0 local torsion, and branch 1 shows a half twist and has local torsion $+1$. The off-diagonal matrix elements are twice the linking number of the period one orbits in the corresponding pair of branches. Since the period-one orbits in these two branches do not link, the off-diagonal matrix elements are 0. The period one orbits in the branches labeled 1 and 2 in Fig. 7(b) have linking number $+1$ so the off-diagonal matrix elements are $T(1,2) = T(2,1) = 2 \times +1$. The array identifies the order (above, below) that the two branches are joined at the branch line, the smaller the value, the closer to the viewer. These two pieces of information, four integers in Fig. 7(a) and eight in Fig. 7(b), serve to determine the topological organization of all the unstable

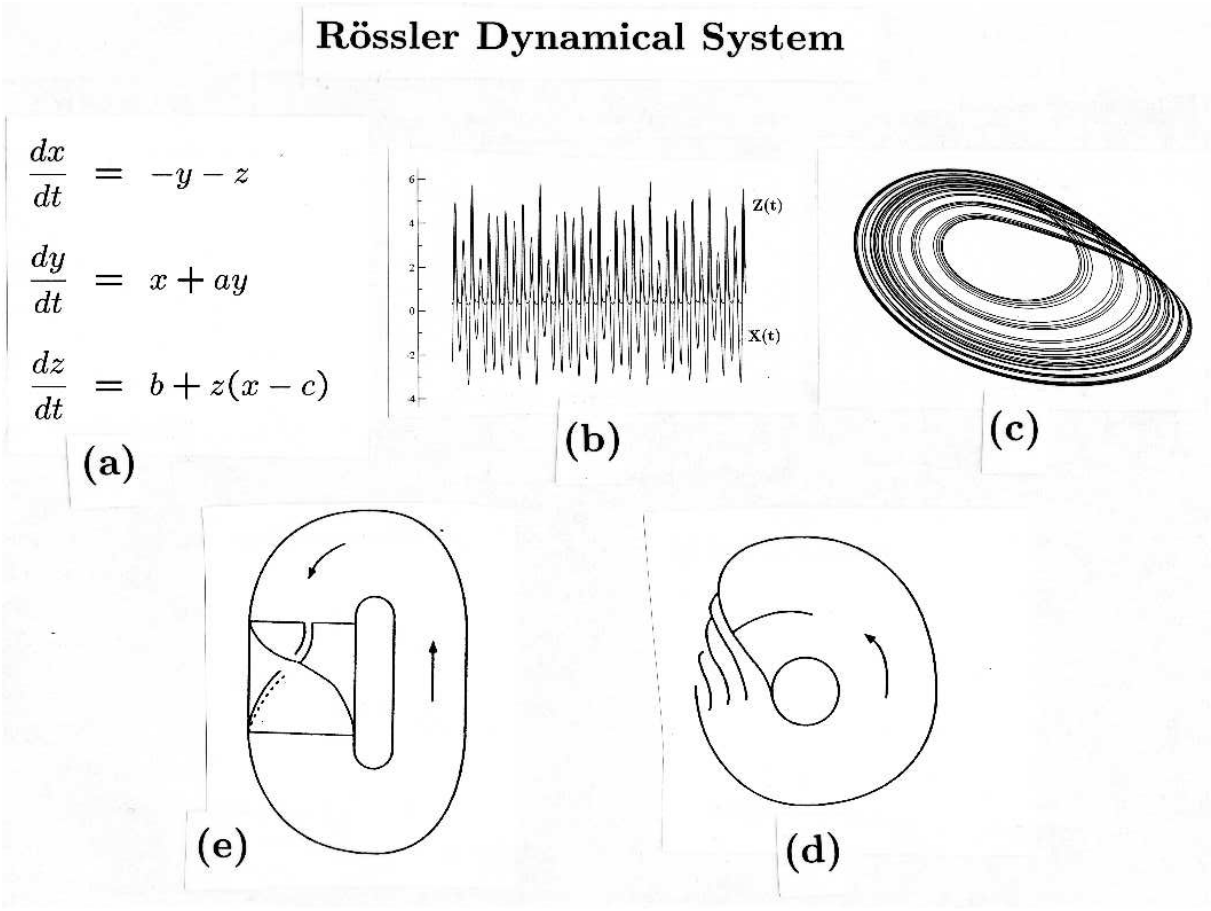

Figure 4: (a) Rössler equations. (b) Time series $z(t)$ and $x(t)$ generated by these equations, and (c) projection of the strange attractor onto the x-y plane. (d) Caricature of the flow and (e) knot holder derived directly from the caricature. Control parameter values $(a, b, c) = (2.0, 4.0, 0.398)$.

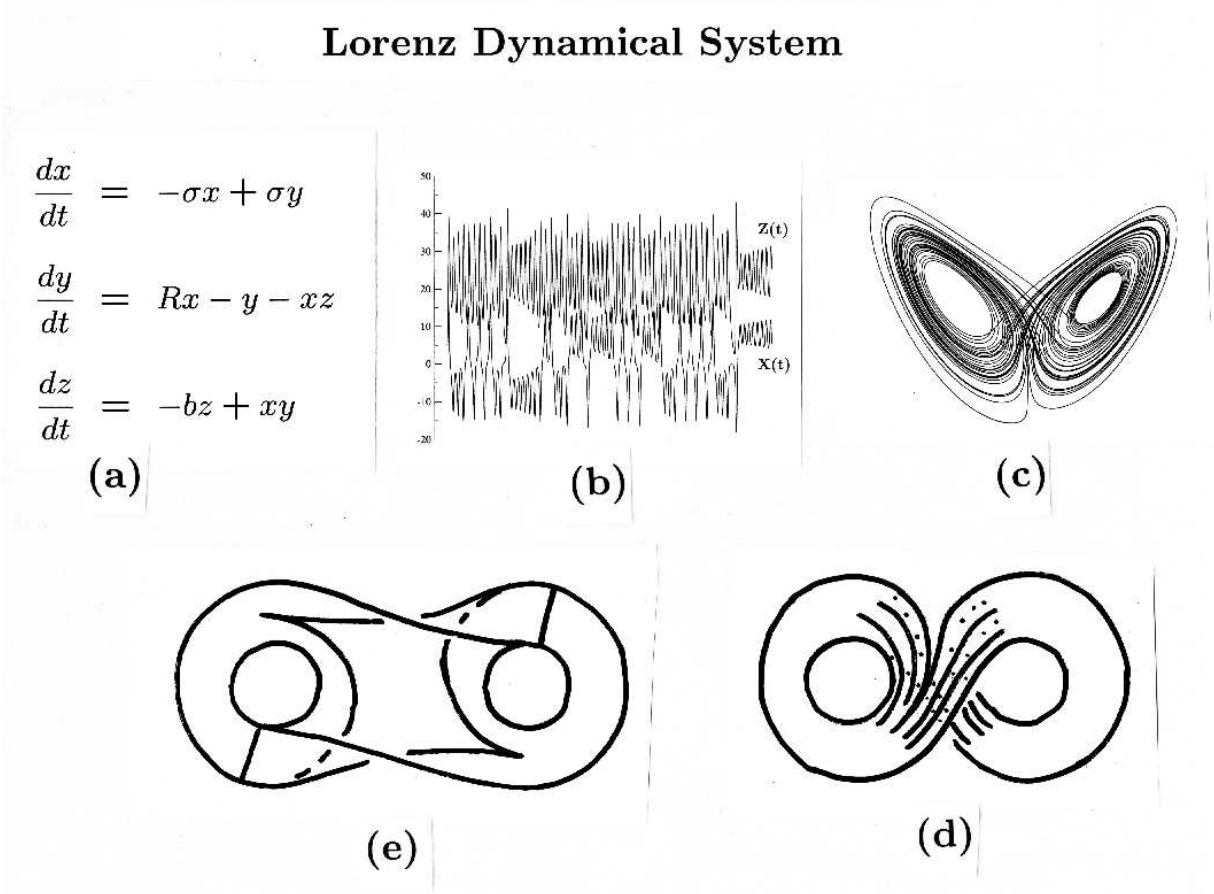

Figure 5: (a) Lorenz equations. (b) Time series $x(t)$ and $z(t)$ generated by these equations, and (c) projection of the strange attractor onto the x-z plane. (d) Caricature of the flow and (e) knot holder derived directly from the caricature by rotating the right hand lobe by π radians. Control parameter values $(R, \sigma, b) = (26.0, 10.0, 8/3)$.

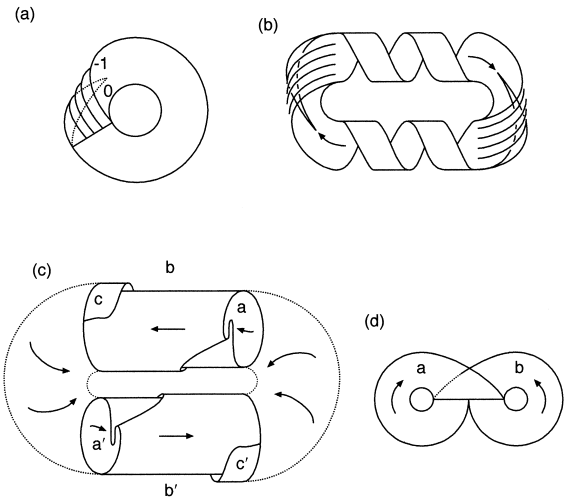

Figure 6: Branched manifolds for four standard sets of equations: (a) Rössler equations; (b) periodically driven Duffing equations; (c) periodically driven van der Pol equations; (d) Lorenz equations. Reprinted with permission from R. Gilmore and M. Lefranc, *The Topology of Chaos*, NY: Wiley, 2002.

periodic orbits in any strange attractor with either branched manifold.

The periodic orbits are identified by a repeating symbol sequence of least period p, which is unique up to cyclic permutation. The symbol sequence consists of a string of integers, sequentially identifying the branches through which the orbit passes. For a branched manifold with two branches, there are two symbols. The number of orbits of period p, $N(p)$, obeys the recursion relation

$$pN(p) = 2^p - \sum_{1=k|p}^{k\leq p/2} kN(k) \tag{3}$$

Table 2 shows the number of orbits of period $p \leq 20$ for the branched manifolds with two and three branches shown in Fig. 7. The number of orbits of period p grows exponentially with p, and the limit $h_T = \lim_{p\to\infty} \log(N(p))/p$ defines the topological entropy h_T for the branched manifold. The limits are $\log(2)$ and $\log(3)$ for the branched manifolds with 2 and 3 branches, respectively. The linking numbers of orbits up to period five in the Smale horseshoe branched manifold are shown in Table 3. The table identifies each of the orbits by its symbol sequence, e.g., 00111.

Tables of linking numbers have been used successfully to identify mechanisms that Nature uses to generate chaotic data. This analysis procedure is called Topological Analysis. Segments of data are identified that closely approximate unstable periodic orbits that exist in the strange attractor. These data segments are then embedded in R^3. Each orbit is given a trial identification (symbol sequence). Their pairwise linking numbers are computed either by counting signed crossings or using the time-parameterized data segments and estimating the integers numerically using the Gauss linking integral

$$\text{Link}(A,B) = \frac{1}{4\pi} \oint \oint \frac{\mathbf{r}_A(t_1) - \mathbf{r}_B(t_2)}{|\mathbf{r}_A(t_1) - \mathbf{r}_B(t_2)|^3} \cdot d\mathbf{r}_A(t_1) \times d\mathbf{r}_B(t_2)$$

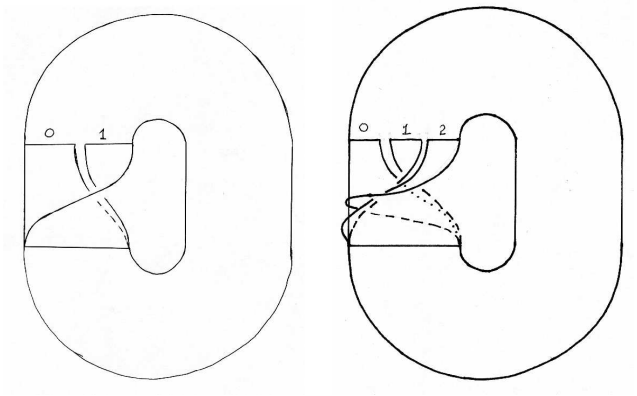

$$\begin{bmatrix} 0 & 0 \\ 0 & 1 \end{bmatrix} \qquad \begin{bmatrix} 0 & 0 & 0 \\ 0 & 1 & 2 \\ 0 & 2 & 2 \end{bmatrix}$$

$$\begin{bmatrix} 0 & -1 \end{bmatrix} \qquad \begin{bmatrix} 0 & -2 & -1 \end{bmatrix}$$

Figure 7: Branched manifolds are described algebraically. The diagonal matrix elements describe the twist of each branch. The off-diagonal matrix elements are twice the linking number of the period-one orbits in each of the two branches. The array describes the order in which the branches are connected at the branch line. (a) Smale horseshoe branched manifold. (b) Beginning of a gateau roulé branched manifold.

Table 2: Number of orbits of period p on the branched manifolds with 2- and 3- branches, shown in Fig. 7. The integers $N_3(p)$ are constructed by replacing 2^p by 3^p in Equ. (3).

Period p	2 Branches $N_2(p)$	3 Branches $N_3(p)$	Period p	2 Branches $N_2(p)$	3 Branches $N_3(p)$
1	2	3	11	186	16104
2	1	3	12	335	44220
3	2	8	13	630	122640
4	3	18	14	1161	341484
5	6	48	15	2182	956576
6	9	116	16	4080	2690010
7	18	312	17	7710	7596480
8	30	810	18	14532	21522228
9	56	2184	19	27954	61171656
10	99	5880	20	52377	174336264

Table 3: Linking numbers of orbits to period five in the Smale horseshoe branched manifold with zero global torsion.

		0	1	2_1	3_1	3_1	4_1	4_2	4_2	5_1	5_1	5_2	5_2	5_3	5_3
	0	0	0	0	0	0	0	0	0	0	0	0	0	0	0
	1	0	0	1	1	1	2	1	1	2	2	2	2	1	1
2_1	01	0	1	1	2	2	3	2	2	4	4	3	3	2	2
3_1	011	0	1	2	2	3	4	3	3	5	5	5	5	3	3
3_1	001	0	1	2	3	2	4	3	3	5	5	4	4	3	3
4_1	0111	0	2	3	4	4	5	4	4	8	8	7	7	4	4
4_2	0011	0	1	2	3	3	4	3	4	5	5	5	5	4	4
4_2	0001	0	1	2	3	3	4	4	3	5	5	5	5	4	4
5_1	01111	0	2	4	5	5	8	5	5	8	10	9	9	5	5
5_1	01101	0	2	4	5	5	8	5	5	10	8	8	8	5	5
5_2	00111	0	2	3	5	4	7	5	5	9	8	6	7	5	5
5_2	00101	0	2	3	5	4	7	5	5	9	8	7	6	5	5
5_3	00011	0	1	2	3	3	4	4	4	5	5	5	5	4	5
5_3	00001	0	1	2	3	3	4	4	4	5	5	5	5	5	4

(4)

This table of experimental integers is compared with the table of linking numbers for orbits with the same symbolic name on a trial branched manifold. This procedure serves to identify the branched manifold and refine the symbolic identifications of the experimental orbits, if necessary. This procedure is vastly overdetermined. For example, the linking numbers of only three low period orbits serve to identify the four pieces of information required to specify a branched manifold with two branches. Since six or more surrogate periodic orbits can typically be extracted from experimental data, providing $\begin{pmatrix} 6 \\ 2 \end{pmatrix} = 15$ or more linking numbers, this Topological Analysis procedure has built-in self-consistency checks, unlike analysis procedures based on geometric and dynamical tools.

4 Basis Sets of Orbits

A branched manifold determines the topological organization of all the periodic orbits that it supports. Whenever a low dimensional strange attractor is subjected to a Topological Analysis, it is always the case that fewer periodic orbits are present and identified than are allowed by the branched manifold that classifies it. This is the case for strange attractors generated by experimental data as well as strange attractors generated by ordinary differential equations. The full spectrum occurs only in the hyperbolic limit, which has never been seen.

The orbits that are present are organized exactly as in the hyperbolic limit — that is, as determined by the underlying branched manifold. As control parameters change, the strange attractor undergoes changes ("perestroikas"). New orbits are created and/or old orbits are annihilated in direct or inverse period-doubling and saddle-node bifurcations. The orbits that are present are always organized as determined by the branched manifold. Orbits are not created or annihilated independently of each other. Rather, there is a partial order ("forcing order") involved in orbit creation and annihilation. This partial order is poorly understood for general branched manifolds. It is much better understood for the two-branch Smale horseshoe branched manifold.

The forcing diagram for this branched manifold is shown in Fig. 8 for orbits up to period eight.

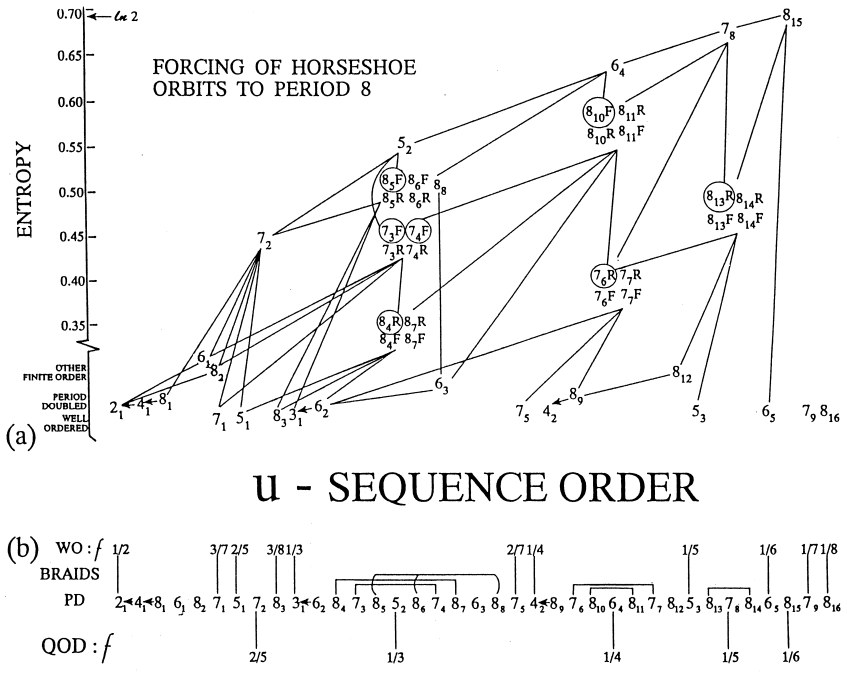

Figure 8: Forcing diagram for orbits up to period eight in the Smale horseshoe branched manifold. Below is the sequence ("universal order") in which orbits are created in the highly dissipative limit, which is the logistic map.

It is typically the case that the existence of one orbit in a strange attractor forces the presence of a spectrum of additional orbits. Forcing is transitive, so if orbit A forces orbit B ($A \Rightarrow B$) and B forces C, than A forces C: if $A \Rightarrow B$ and $B \Rightarrow C$ then $A \Rightarrow C$. For this reason it is sufficient to show only the first order forcing in this figure. The orbits shown are labeled by their period and the order in which they are created in a particular highly dissipative limit of the dynamics: the logistic map (U-sequence order in Fig. 8). For example, 5_2 describes the second (pair) of period-five orbits created in the logistic map in the transition from simple, nonchaotic behavior to fully chaotic (hyperbolic) behavior.

The orbits in the forcing diagram are organized according to their one-dimensional entropy (horizontal axis, U-sequence order) and their two-dimensional entropy (vertical axis). Nonchaotic ("laminar") behavior occurs at the lower left of this figure, where both entropies are zero. Fully chaotic behavior occurs at the upper right, where both entropies are ln(2). As control parameters change, a dynamical system that can exhibit chaos generated by a stretch and fold mechanism follows a path in the forcing diagram from the lower left to the upper right. Each such path is a "route to chaos." The Smale horseshoe mechanism exhibits many different routes to chaos: Each follows a different path in the forcing diagram.

The state of a strange attractor at any stage in its route to chaos can be specified by a "basis set of orbits." This is a set of orbits whose presence forces the existence of all other orbits that can concurrently be found in the attractor, up to any finite period. The basis set of orbits can be

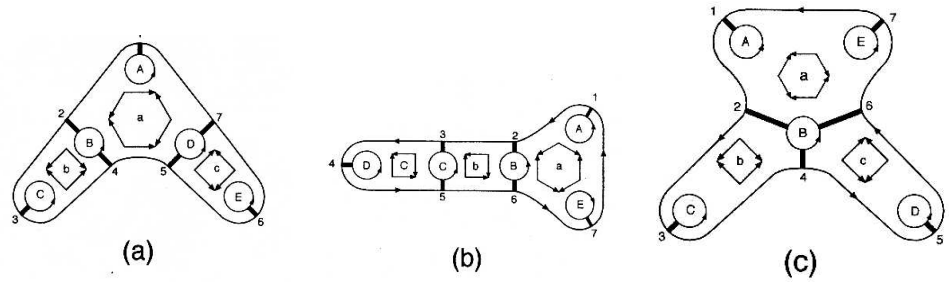

ABCBDED
abbacca

ABCDCBE
abccbaa

ABCBDBE
abbccaa

Figure 9: Three inequivalent canonical forms of genus eight are shown. Each is identified by a "period 7 orbit" and its dual.

constructed algorithmically. The algorithm is as follows. Write down all the orbits that are present in order of increasing two-dimensional entropy from left to right. For orbits with the same two-dimensional entropy, order by increasing one-dimensional entropy. Remove the "highest" (rightmost) orbit from this list, together with all the orbits that it forces. This is the first basis orbit. Of the orbits remaining, again remove the rightmost and all the orbits that it forces. This is the second basis orbit. Continue until all orbits have been removed. For any finite period, this algorithm terminates because there is only a finite number of orbits. For example, if the orbit 5_2 is present as well as all orbits with lower one-dimensional entropy, the basis set is $8_7R, 7_6, 7_4F, 8_6F, 8_8, 5_2$. As control parameters change, a strange attractor undergoes perestroikas that are quantitatively determined by changes in the basis sets of orbits.

5 Bounding Tori

As experimental conditions or control parameters change, strange attractors can undergo "grosser" perestroikas than those that can be described by a change in the basis set of orbits. This occurs when new orbits are created that cannot be contained on the initial branched manifold – for example, when orbits are created that must be described by a new symbol. This is seen experimentally in the transition from horseshoe type dynamics to gateau roulé ("jelly roll") type dynamics. This involves the addition of a third branch to the branched manifold with two branches, as shown in Figs. 7(a) and 7(b). Strange attractors can undergo perestroikas described by the addition of new branches to, or deletion of old branches from, a branched manifold. These perestroikas are in a very real sense "grosser" than the perestroikas that can be described by changes in the basis sets of orbits on a fixed branched manifold.

There is a structure that provides constraints on the allowed bifurcations of branched manifolds (creation/annihilation of branches) that is analogous to the constraints that a branched manifold provides on the bifurcations and topological organization of the periodic orbits that can exist on it. This structure is called a bounding torus.

Bounding tori are constructed as follows. The semiflow on a branched manifold is "inflated" or "blown up" to a flow on a thin open set in R^3 containing this branched manifold. The boundary of this open set is a two-dimensional surface. Such surfaces have been classified. They are uniquely

tori of genus g, $g = 0$ (sphere), $g = 1$ (tire tube), $g = 2, 3, \ldots$. The torus of genus g has Euler characteristic $\chi = 2 - 2g$. The flow is into this surface. The flow, restricted to the surface, exhibits a singularity wherever it is normal to the surface. At such singularities the stability is determined by the local Lyapunov exponents: $\lambda_1 > 0$ and $\lambda_3 < 0$, since the flow direction ($\lambda_2 = 0$) is normal to the surface. As a result all singularities are saddles, so by the Poincaré-Hopf theorem the number of singularities is strongly related to the genus. The number is $2(g-1)$.

The flow, restricted to the genus-g surface, can be put into canonical form and these canonical forms can be classified. The classification involves projection of the genus-g torus onto a two-dimensional surface. The planar projection consists of a disk with outer boundary and g interior holes. All singularities can be placed on the interior holes. The flow on the interior holes without singularities is in the same direction as the flow on the exterior boundary. Interior holes with singularities have an even number, 4, 6, ... Some canonical forms are shown in Fig. 9.

Poincaré sections have been used to simplify the study of flows in low dimensional spaces by effectively reducing the dimension of the dynamics. In three dimensions a Poincaré surface of section for a strange attractor is a minimal two-dimensional surface with the property that all points in the attractor intersect this surface transversally an infinite number of times under the flow. The Poincaré surface need not be connected and in fact is often not connected.

The Poincaré section for the flow in a genus-g torus consists of the union of $g-1$ disjoint disks ($g \geq 3$) or is a single disk ($g = 1$). The locations of the disks are determined algorithmically, as shown in Fig. 9. The interior circles without singularities are labeled by capital letters $A, B, C, \ldots$ and those with singularities are labeled with lower case letters $a, b, c, \ldots$. The components of the global Poincaré surface of section are numbered sequentially 1, 2, ... , $g-1$, in the order they are encountered when traversing the outer boundary in the direction of the flow starting from any point on that boundary. Each component of the global Poincaré surface of section connects (in the projection) an interior circle without singularities to the exterior boundary. There is one component between each successive encounter of the flow with holes that have singularities. Heavy lines are used to show the location of the seven components of the global Poincaré surface of section for each of the three inequivalent genus-8 canonical forms shown in Fig. 9. The structure of the flow is summarized by a transition matrix. For the canonical form shown in Fig. 9(c) the transition matrix is

$$T = \begin{bmatrix} 1 & 1 & 0 & 0 & 0 & 0 & 0 \\ 0 & 0 & 1 & 1 & 0 & 0 & 0 \\ 0 & 0 & 1 & 1 & 0 & 0 & 0 \\ 0 & 0 & 0 & 0 & 1 & 1 & 0 \\ 0 & 0 & 0 & 0 & 1 & 1 & 0 \\ 0 & 1 & 0 & 0 & 0 & 0 & 1 \\ 1 & 0 & 0 & 0 & 0 & 0 & 1 \end{bmatrix}$$

where $T_{i,j} = 1$ if the flow can proceed directly from component i to component j, 0 otherwise.

Bounding tori, dressed with flows, can be labeled. In fact, two dual labeling schemes are possible. Following the outer boundary in the direction of the flow, one encounters: the $g-1$ components of the global Poincaré surface of section sequentially; the interior holes without singularities at least once each; and the interior holes with singularites at least twice each. The canonical form (genus-g torus dressed with a flow) on the genus-8 bounding torus shown in Fig. 9(a) can be labeled by the sequence in which the holes without singularities are encountered ($ABCBDED$) or the order in which the holes with singularities are encountered (*abbacca*). Both sequences contain $g-1$ symbols. These labels are unique up to cyclic permutation.

Symbol sequences for canonical forms for bounding tori act in many ways like symbol sequences

Table 4: Number of canonical bounding tori as a function of genus, g.

g	$N(g)$	g	$N(g)$	g	$N(g)$
3	1	9	15	15	2211
4	1	10	28	16	5549
5	2	11	67	17	14290
6	2	12	145	18	36824
7	5	13	368	19	96347
8	6	14	870	20	252927

for periodic orbits on branched manifolds. Although there is a 1:1 corresondence between bounded closed two-dimensional surfaces in R^3 and genus, g, the number of canonical forms grows rapidly with g, as shown in Table 4. In fact, the number, $N(g)$, grows exponentially and can even be assigned an entropy:

$$\lim_{g\to\infty} \frac{\log(N(g)}{g-1} = \log(3) \tag{5}$$

In some sense, canonical forms that constrain branched manifolds within them behave like branched manifolds that constrain periodic orbits on them.

Every strange attractor that has been studied in R^3 has been described by a canonical bounding torus that contains it. This classification is shown in Table 5.

Table 5: All known strange attractors of dimension $d_L < 3$ are bounded by one of the standard dressed tori. Dual labels for the bounding tori depend on $g-1$ symbols describing either holes without singularities or holes with singularities.

Strange Attractor	Holes W/O Singularites	Holes W Singularities	genus
Rossler, Duffing, Burke and Shaw	A		1
Various Lasers, Gateau Roule	A		1
Neuron with Subthreshold Oscillations	A		1
Shaw-van der Pol	A		1
Lorenz, Shimizu-Morioka, Rikitake	AB	aa	3
$\mathcal{C}_2$ Covers of Rossler	AB	a^2	3
$\mathcal{C}_2$ Cover of Lorenz$^{(a)}$	$ABCD$	a^4	5
$\mathcal{C}_2$ Cover of Lorenz$^{(b)}$	$ABCB$	$abba$	5
$2 \to 1$ Image of Fig. 8 Branched Manifold	$ABCB$	$ab(ab)^{-1}$	5
Fig. 8 Branched Manifold	$AEBECEDE$	$a^2b^2c^2d^2$	9
$\mathcal{C}_n$ Covers of Rossler	$AB\cdots N$	a^n	$n+1$
$\mathcal{C}_n$ Cover of Lorenz$^{(a)}$	$AB\cdots(2N)$	a^{2n}	$2n+1$
$\mathcal{C}_n$ Cover of Lorenz$^{(b)}$	$(AZ)(BZ)\cdots(NZ)$	$a^2b^2\cdots n^2$	$2n+1$
Multispiral Attractors	$A(B\ldots M)N(B\ldots M)^{-1}$	$(ab\ldots m)(ab\ldots m)^{-1}$	$2m+1$

$^{(a)}$ Rotation axis through origin.
$^{(b)}$ Rotation axis through one focus.

Branched manifold perestroikas are constrained by bounding tori as follows. Each branch line of

any branched manifold can be moved into one of the $g-1$ components of the global Poincaré surface of section. Any branched manifold contained in a genus-g bounding torus ($g \geq 3$) must have at least one branch between each pair of components of the global Poincaré surface of section between which the flow is allowed, as summarized by the canonical form's transition matrix. New branches can only be added in a way that is consistent with

- the canonical form's transition matrix
- continuity requirements
- the no intersection condition

In the simplest case, $g = 1$, a third branch can be added to a branched manifold with two branches only if its local torsion differs by ± 1 from the adjacent branch. In addition, the ordering of the new branch must be consistent with the continuity and no intersection (ODE uniqueness theorem) requirements.

6 Embeddings of Bounding Tori

The last level of topological structure needed for the classification of strange attractors in R^3 describes their embeddings in R^3. The classification using genus-g bounding tori is intrinsic — that is, the canonical form shows how the flow looks from inside the torus. Strange attractors, and the tori that bound them, are actually embedded in R^3. For a complete classification we must specify not only the canonical form but also how this form sits in R^3.

This program has not yet been completed, but we illustrate with the genus-one bounding torus in Fig. 10. This figure shows the canonical form at the top, and two different embeddings of it in R^3. The embedding on the left is unknotted. The embedding on the right is knotted like a figure 8 knot. Extrinsic embeddings of genus-one tori are described by tame knots in R^3, and tame knots can be used as "centerlines" for extrinsically embedded genus-one tori. Higher genus ($g \geq 3$) canonical forms — intrinsic genus-g tori dressed with a canonical flow — have a larger (but discrete) variety of extrinsic embeddings in R^3.

7 The Embedding Question

The mechanism that Nature uses to generate chaotic behavior in physical systems is not directly observable, and must be deduced by examining the data that are generated. Typically the data consist of a single scalar time series that is discretely recorded: $x_i,\ i = 1, 2, \ldots$. In order to exhibit a strange attractor, a mapping of the data into R^N must also be constructed. If the attractor is low dimensional ($d < 3$) one can hope that a mapping into R^3 can be constructed that exhibits no self-intersections or other degeneracies. Such a map is called an embedding. Once an embedding in R^3 is available, a Topological Analysis can be carried out. The analysis reveals the mechanism that underlies the creation of the embedded strange attractor.

But how do you know that the mechanism that generates the observed, embedded strange attractor has anything to do with the mechanism Nature used to generate the experimental data?

If the embedding is contained in a genus-one bounding torus, then the topological mechanism that generates the data, as defined by some unknown branched manifold $\mathcal{BM}_{\rm EXP}$, and the topological mechanism that is identified from the embedded strange attractor $\mathcal{BM}_{\rm EMB}$, are identical up to three degrees of freedom:

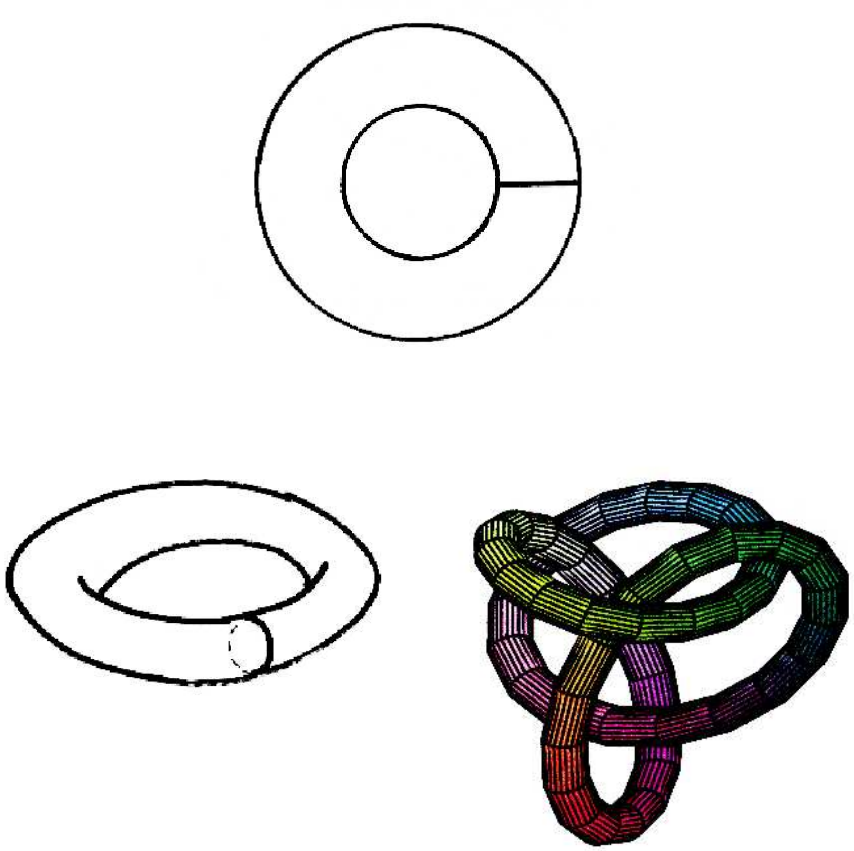

Figure 10: (a) Canonical form for genus-one bounding torus. Extrinsic embeddings of the torus into R^3 that are (b) unknotted and (c) knotted like the figure 8 knot.

- parity
- global torsion
- knot type.

As a result, in this case (genus-one) Topological Analysis of embedded data does reveal Nature's hidden secrets.

8 Further Reading

R. Gilmore and M. Lefranc, *The Topology of Chaos, Alice in Stretch and Squeezeland*, NY: Wiley, 2002.

N. B. Tufillaro, T. Abbott, and J. Reilly, *An Experimental Approach to Nonlinear Dynamics and Chaos*, Reading, MA: Addison-Wesley, 1992.

H. G. Solari, M. A. Natiello, and G. B. Mindlin, *Nonlinear Physics and its Mathematical Tools*, Bristol: IOP Publishing, 1996.

R. Gilmore, Topological analysis of chaotic dynamical systems, *Reviews of Modern Physics* **70**, (4), 1455-1529 (1998).

J.-P. Eckmann and D. Ruelle, Ergodic theory of chaos and strange attractors, *Reviews of Modern Physics* **57**(3), 617-656 (1985).

R. Gilmore and X. Pei, The topology and organization of unstable periodic orbits in Hodgkin-Huxley models of receptors with subthreshold oscillations, in: *Handbook of Biological Physics, Vol. 4, Neuro-informatics, Neural Modeling*, (F. Moss and S. Gielen, Eds.), Amsterdam, North Holland, 2001, pp. 155-203.

E. Ott, *Chaos in Dynamical Systems*, Cambridge: University Press, 1993.

R. Abraham and C. D. Shaw, *Dynamics: The Geometry of Behavior (Studies in Nonlinearity)* (Second Edition), Reading, MA: Addison-Wesley, 1992.